Research Square

Preprints are preliminary reports that have not undergone peer review.
They should not be considered conclusive, used to inform clinical practice,
or referenced by the media as validated information.

Mechanistic Insights into the Binding Stability and Covalent Inhibition of Lactone- Based Pancreatic Lipase Inhibitors Using Molecular Dynamics and Binding-Pose Metadynamics

Sanjay Kottekad
CSIR-Central Food Technological Research Institute
Usharani Dandamudi
ushad.cftri@csir.res.in

CSIR-Central Food Technological Research Institute

Research Article

Keywords: Pancreatic Lipase Inhibition, Obesity, Microbial Lactones, β-Lactone Warhead, Covalent Inhibition, Reversible Covalent Inhibition, Binding Pose Metadynamics, Anti-Obesity Treatment, Lipid Digestion

Posted Date: November 4th, 2026

DOI: https://doi.org/10.21203/rs.3.rs-11271846/v1

License: This work is licensed under a Creative Commons Attribution 4.0 International License.
Read Full License

Additional Declarations: No competing interests reported.

Abstract

Pancreatic lipase (PL) is a key digestive enzyme involved in dietary lipid hydrolysis and represents an important target for the development of lipid-lowering agents. In the present study, the binding dynamics, stability, and covalent inhibition characteristics of microbial and synthetic lactone-based PL inhibitors were investigated using molecular docking, molecular dynamics (MD) simulations, binding free-energy calculations, binding-pose metadynamics, and water-tunnel analysis. The inhibitors predominantly occupied the S1–S2 region of the catalytic site in the open conformation of PL, where their structural features, including the β-lactone ring, amide-containing substituents, and hydrophobic alkyl chains, contributed to ligand recognition and stabilization. Comparative binding free-energy calculations using the Amber ff14SB and OPLS3e force fields showed that Esterastin and Orlistat exhibited the most favourable computed binding energetics, driven predominantly by electrostatic and van der Waals interactions. Binding-pose metadynamics further demonstrated enhanced stability of the covalently bound inhibitor complexes and provided insight into differences in their conformational changes and residence time within the catalytic pocket. Further, the unbinding of inhibitor dependence through dynamic solvent pathways connecting the protein surface to the catalytic region and indicated that water molecules in the vicinity of the catalytic residue Ser153 may influence hydrolytic accessibility and thereby modulate the reversibility of lactone inhibition. Collectively, these findings provide a molecular-level understanding of how lactone architecture, active-site interactions, covalent-complex stability, and catalytic-site hydration govern binding affinity to pancreatic lipase inhibition.

1. Introduction

Covalent inhibition is an important strategy in enzyme regulation and drug design, particularly for enzymes that contain highly nucleophilic catalytic residues. In such systems, electrophilic functional groups, often referred to as warheads, react with active-site residues to form stable or reversible covalent enzyme-inhibitor complexes.[1] Serine hydrolases are especially suitable targets for this mode of inhibition because their catalytic serine residue participates directly in nucleophilic attack during substrate hydrolysis.[2] Pancreatic lipase (PL), a digestive serine hydrolase responsible for dietary lipid hydrolysis, is a clinically relevant example of an enzyme that can be inhibited through covalent modification of its catalytic serine.[1] The anti-obesity drug orlistat inhibits PL by using its beta-lactone warhead to form a covalent ester bond with catalytic Ser153, thereby blocking triglyceride hydrolysis and reducing intestinal fat absorption. This covalent inhibition mechanism provides a useful framework for understanding how lactone-based inhibitors interact with PL and how structural variations among microbial and synthetic lactones may influence binding stability, reversibility, and inhibitory potency.

Excessive fat intake combined with a sedentary lifestyle can significantly disrupt lipid homeostasis in the body, leads to an inefficiency of dietary lipid metabolism and utilisation.[3] This can contribute to adipogenesis, the process by which new cells are formed, to store the excess energy as fat, leading to overweight and obesity.[4,5] Obesity is associated with a range of comorbidities including type 2 diabetes,

cardiovascular disease and metabolic syndrome.[3] Among the various anti-obesity targets, pancreatic lipase (PL) stands out as a key player in the exogenous pathway of dietary lipid digestion and absorption. PL (E.C. 3.1.1.3) is an essential enzyme produced by the pancreas that plays a critical role in hydrolysing more than 70% of neutral triglycerides in the small intestine, into absorbable monoglycerides (MAG) and free fatty acids (FFA).[6] Targeting PL with specific inhibitors can reduce the enzymatic breakdown of triglycerides, decrease the absorption of dietary fats, and ultimately contribute to weight management and the treatment of obesity.[3]

PL is composed of 449 amino acid residues and function effectively at the lipid-water interface in the small intestine.[6,7] This involves the opening of its amphipathic lid region (237–262), hydrophilic β-5 loop (75–85), and hydrophobic β-9 (205–223) to draw lipid droplets from emulsified dietary lipids into the active site groove.[5,6] This process is facilitated by the cofactor, colipase (CL), which stabilizes the open conformation of the enzyme by forming hydrogen bonds, anchoring the lipase at the interface, and aiding in lipolysis.[5] As a member of the serine esterase family, PL possess a classical catalytic triad composed of serine (S153), histidine (H264), and aspartic acid (D177) residues.[7] During catalysis, Ser153 acts as the nucleophile and attacks the ester bond of the lipid substrate, forming a tetrahedral intermediate that is stabilized by the oxyanion hole. Subsequent hydrolysis releases the lipid products and regenerates the active enzyme.[7] Structural studies have provided important insight into covalent inhibition of PL. The crystal structure of human PL complexed with the synthetic organophosphate inhibitor C11 alkyl phosphonate, also known as MUP, shows covalent modification of the catalytic serine within the active site.[1] This structure illustrates how the catalytic pocket, oxyanion hole, lid region, and beta-loop architecture cooperate to stabilize inhibitor binding and block access to the hydrolytic machinery. Similarly, orlistat forms a covalent ester bond with Ser153 through its beta-lactone warhead.[8] The resulting enzyme-inhibitor complex prevents triglyceride hydrolysis by occupying the catalytic site and disrupting the normal acyl-enzyme catalytic cycle. Interestingly, orlistat inhibition has been described as stable at the lipid-water interface, while reversible behavior has been observed under aqueous conditions in the absence of substrate, suggesting that water accessibility near the catalytic site may influence the reversibility of lactone-mediated covalent inhibition.[8,9]

Microbial lactones were among the earliest reported PL inhibitors and remain valuable scaffolds for understanding structure-dependent enzyme inhibition.[10–14] Scheme 1 illustrates the structures of 13 PL inhibitors derived from microbial and synthetic origin, along with their reported IC_{50} by which they inhibit PL *in vitro*. Esterastin, a secondary metabolite from actinomycetes, was identified as a highly potent PL inhibitor with an IC_{50} of 0.00039 uM.[10] Its structure contains long hydrophobic alkyl chains, an amide branch, and a beta-lactone warhead, structural features that are also observed in several other potent lactone inhibitors. Subsequent studies identified ebelactone A, ebelactone B, and valilactone as microbial beta-lactone inhibitors of PL[11,12] (Scheme 1). Their structures are smaller yet similar to Esterastin, with one short and one long alkyl chain along with a β-lactone ring as the warhead (Scheme 1).[11] Valilactone showed inhibition comparable to esterastin, probably because of similarities in

hydrophobic chain architecture and lactone-based reactivity.[12] Lipstatin, isolated from *Streptomyces toxytricini*, later became especially important because its hydrogenated derivative, tetrahydrolipstatin or orlistat, is the only FDA-approved anti-obesity drug that targets PL.[13,14]

Despite the clinical success of orlistat, its long-term use is associated with gastrointestinal adverse effects, including diarrhoea, nausea, bloating, dyspepsia, and fat-soluble vitamin malabsorption. These limitations have encouraged the search for alternative PL inhibitors with improved selectivity, potency, and tolerability. Cetilistat is one such synthetic lactone-based inhibitor and differs structurally from orlistat by containing a delta-lactone instead of a beta-lactone.[15] In addition, other microbial lactones such as panclicins and vibralactone have shown PL inhibitory activity, further suggesting that lactone-based scaffolds can be chemically diverse while retaining inhibitory potential.[16,17] However, although several microbial and synthetic lactones have demonstrated PL inhibition in vitro, their detailed binding mechanisms remain incompletely understood.

A major unresolved question is how different lactone scaffolds engage the PL active site through non-covalent recognition and covalent bond formation. Important structural features such as the lactone warhead, alkyl chain length, amide branch, hydrophobic packing, catalytic Ser153 proximity, oxyanion-hole stabilization, and water accessibility may collectively determine whether an inhibitor forms a stable covalent complex or displays reversible covalent behavior. Therefore, computational approaches can provide useful atomic-level insight into ligand orientation, binding stability, active-site conformational dynamics, and catalytic-site accessibility. In the present study, molecular docking, molecular dynamics simulations, binding free energy analysis, binding-pose metadynamics, and tunnel pathway analysis were employed to investigate microbial and synthetic lactone-based PL inhibitors. This work aims to clarify how structural variations among lactone inhibitors influence their binding stability and covalent inhibition mechanisms, thereby supporting the rational design of improved PL-targeted inhibitors.

2. Computational Details

2.1. Preparation of Pancreatic Lipase and Inhibitors Structures

Protein

Crystal structure of Human pancreatic lipase (PL), 1LPB was retrieved from RCSB, PDB.[18,19,20] The co-crystallized C11 alkyl phosphonate inhibitor in the 1LPB was removed and the pKa values of the protonated and deprotonated PL residues were obtained from PROPKA 2.0.[21] The protonation states of histidine were corrected after a thorough visual inspection of the structure using Visual Molecular Dynamics (VMD).[22] Missing hydrogens were added using the Leap module of Amber 20 with Amber ff14SB force field parameters.[23]

Inhibitors

The structures of 11 microbial lactones, and the synthetic lactones Orlistat and Cetilistat were obtained from PubChem database.[24] Parameters for the inhibitors were generated using the antechamber module of Amber using general amber force field (GAFF).[23] Partial atomic charges and missing parameters were obtained using the RESP method with HF/6-31G* geometry optimization in the Gaussian 16 package.[25] A detailed work flow was provided in Scheme 2.

2.2. Molecular Docking of Lactones Towards PL

Molecular docking was performed for the 13 lactones with PL using AutoDock Vina module in UCSF Chimera.[26,27] The PL active site was encapsulated using the grid box dimension 10.3155 X 26.1696 X 44.8469 A° with a size of 26.0531 X 22.34 X 25.0309 A°. Using Broyden-Fletcher-Goldfarb-Shanno (BFGS) algorithm for iterative local search optimizations, nine docking poses were generated for each inhibitor. The molecular docking results were subsequently analysed to identify the most favourable binding conformations, determined by the lowest binding energy values (in kcal/mol) and interaction with the active site residues.

2.3. Molecular Dynamics Simulation of PL-Lactone Complex

To assess the stability of protein-lactone complexes and identify key steric and noncovalent interactions, 100 ns molecular dynamics simulations were performed using Amber 20.[23] The complexes were neutralized with Na^+ and Cl^- counterions and solvated in a 12 Å octahedral box, extending from the protein's peripheral residues. Initially, the solvated protein-inhibitor complex was minimized for 10,000 cycles with restraints on the protein to equilibrate water and hydrogen bonding interactions. Initially, residues 1 to 539 of the protein were restrained with a force constant, 500.0 kcal/mol·Å². This was followed by relaxation using a combination of steepest descent and conjugate gradient methods to optimize the hydrogen bond network and address any steric clashes involving water molecules.[28,29] The system was then subjected to Langevin dynamics to increase the temperature from 100 K to 300 K over a short period (50 ps) under NVT conditions (constant volume and temperature). The density of the system was normalized under NPT conditions (constant pressure and temperature) for 1 ns, with pressure and temperature maintained at 1.0 atm and 300 K, respectively. Once a uniform density was achieved, the system was equilibrated for an additional 3 ns with a pressure relaxation time of 2.0 ps. A subsequent 100 ns production run was conducted for detailed analysis of the enzyme-inhibitor complex. The pressure and temperature roughout the simulation, were regulated using Berendsen barostat and Langevin thermostat models.[30,31] The SHAKE algorithm was employed to constrain hydrogen atoms, and electrostatic interactions were calculated using the Particle Mesh Ewald (PME) method.[32,33] The MD trajectories were analysed with the VMD package.[22] Root mean square deviation (RMSD), root mean square fluctuation (RMSF), number of hydrogen bonds and water molecules in the MD trajectory were analysed using the CPPTRAJ module.[23] Trajectory clustering was performed using a hierarchical agglomerative approach within CPPTRAJ.

All the simulations were performed in a Linux workstation, graphics were prepared using PyMOL 1.7 and GraphPad Prism.[34,35]

2.4. Estimation of Binding Free Energy and Per-Residue Decomposition of Binding Energy

Binding free energy

The relative binding free energies of the PL-Lactone complexes were calculated with the MMGBSA (Molecular Mechanics Generalized Born Surface Area) module, available in Amber20.[23] Topology parameters for the ligand (lactone), receptor (PL), and complex (PL-lactone) were prepared using the ff14SB force field with the Leap module in Amber20.[23] The Born radii were assigned using the mbondi2 parameters, as defined by the GBOBC2 model (igb = 5). Default dielectric constants of 1.0 for the interior and 80 for the exterior were applied. The solvation free energy calculation using MMGBSA follows a thermodynamic cycle involving the bound complex and the unbound ligand and receptor, considering both solvent and gas phases. The resultant solvation free energy can be computed using the formula provided below.

$$\Delta \mathrm{G}^{0}_{\mathrm{bind,solv}} = \Delta \mathrm{G}^{0}_{\mathrm{bind,vaccum}} + \Delta \mathrm{G}^{0}_{\mathrm{solv,complex}} - (\Delta \mathrm{G}^{0}_{\mathrm{solv,inhibitor}} + \Delta \mathrm{G}^{0}_{\mathrm{solv,protein}})$$

In this context, $\Delta \mathrm{G}^{0}_{\mathrm{bind,solv}}$ represents the difference in solvation free energy between the inhibitor bound to the PL protein active site and the unbound inhibitor. This includes $\Delta \mathrm{G}^{0}_{\mathrm{bind,vaccum}}$, which is the free energy difference between the bound and unbound forms of the inhibitor and protein in a vacuum. Additionally, $\Delta \mathrm{G}^{0}_{\mathrm{solv,complex}}$, $\Delta \mathrm{G}^{0}_{\mathrm{solv,inhibitor}}$ and $\Delta \mathrm{G}^{0}_{\mathrm{solv,protein}}$ denote the differences in solvation free energies for the complex, inhibitor, and protein in the solvent, respectively. Also,

$$\Delta \mathrm{G}^{0}_{\mathrm{solv}} = \Delta \mathrm{G}^{0}_{\mathrm{electrostatic}} + \Delta \mathrm{G}^{0}_{\mathrm{hydrophobic}}$$

Here, $\Delta \mathrm{G}^{0}_{\mathrm{solv}}$ represents the solvation free energy, which combines the electrostatic energy ($\Delta \mathrm{G}^{0}_{\mathrm{electrostatic}}$) and the non-electrostatic or hydrophobic energy ($\Delta \mathrm{G}^{0}_{\mathrm{hydrophobic}}$) of the PL-inhibitor system.

Per-Residue Decomposition of Free Energy

Binding free energy contribution of each residue in the PL-Lactone complex were calculated using pairwise per-residue energy decomposition algorithm available in the Amber16.[23] Free energy decomposition was done along with MMGBSA module and it gives the individual energy contribution of each residue which stabilizes the protein-ligand complex. The data was analysed to pull out the residues contributing towards the van der Waals, internal, electrostatic, polar and non-polar solvation energies of the HPL-Lactone complex.

2.5. Covdock Simulation and Binding Energy Estimation for Covalent Docking

Covalent docking

Covalent docking of microbial lactones with the PL's catalytic residue, S153 was performed in Maestro software from Schrödinger's computational platform.[36,37] CovDock algorithm utilizes both Glide and Prime of Maestro to model covalent ligand binding.[38,39] Initially, PL was minimized using Protein Preparation Wizard, hydrogen atoms and missing residues were added, bond orders were assigned, termini were capped, and protonation states were optimized in Maestro.[37] Ligands were prepared using LigPrep, ensuring accurate protonation states and generating force field torsional parameters for structures not covered by normal OPLS3e parameters in Maestro.[37] Later Glide docking was performed to position the pre-reaction form of the ligand (microbial lactones) close to the receptor's (PL) reactive residue, S153, using positional constraints.[38] A maximum of 10 ligand poses are retained and subjected to post-docking minimization. Only those poses with 2.5 GlideScore units of minimum were selected and poses with distances greater than 5 Å from the Cα atom of S153 are discarded. Following this, a covalent bond was formed based on the specified reaction including any changes in bond order and hydrogen abstractions/additions. In our case, Orlistat is known to have nucleophilic attack to hydroxyl functional group of S153 with its β-lactone carbonyl carbon. This will lead to the opening of the β-lactone ring and form an ester linkage leading to the formation of a PL-Orlistat covalent adduct. Therefore, a nucleophilic addition was predefined in the Maestro to recognize the β-lactone group of microbial lactones and performed the necessary postreaction modifications using click chemistry tool in the software. The reactive group on the ligand, β-lactone ring, was identified using a SMARTS pattern. After covalent bonding, the complexes were minimized in the gas phase and clustered by cartesian coordinates, in order to eliminate duplicates and reduce the number of complexes for postprocessing. CovDock simulation was performed to estimate the GlideScores in order to select and rank the PL-lactone covalent complexes.

Binding Energy Estimation of Covdock Complexes

The refined covalent complexes of microbial and synthetic lactones from CovDock simulation were estimated with their free energy of binding using Prime module in the Maestro.[39] The Variable Dielectric Surface Generalized Born model (VSGB) was used to calculate the binding energy by which the lactones are covalently bound with PL.[39] The total binding energy (ΔGBind), expressed in kcal/mol, is calculated by subtracting the individual binding energies of the PL and lactones from the binding energy of the PL-lactone complex.

2.6. Binding Pose Metadynamics (BPMD)

Binding pose metadynamics (BPMD) was performed using the Maestro software from Schrödinger's computational platform to further understand the strength of covalent binding of microbial lactones with PL.[36,37,40,41] The covalent docked complexes of protein-inhibitors were taken for BPMD simulation. BPMD is a variant of metadynamics simulation in which ten independent metadynamics runs (each 10 ns) were performed. These runs utilize the RMSD of ligand (microbial lactones) heavy atoms from their initial positions as the collective variables (CVs).[40,41] A gaussian bias factor was applied on the CVs of inhibitors during the metadynamics phase, constitute a gaussian hill height of 0.05 kcal/mol and gaussian width of 0.02, at 300 K. Initially, the system was solvated using SPC/E water molecules, and subjected to several minimization steps at 300 K to resolve any initial structural strains or bad contacts. Followed by an equilibration step of 0.5 ns using unbiased MD simulation. The final equilibration snapshot was used as the source for the subsequent ten metadynamics production phases of 10 ns each. BPMD, as described by Clark et al.; 2016, involves running multiple short metadynamics simulations instead of long ones till the free energy surface is fully aligned.[42] In this approach, several candidate poses are perturbed throughout the simulations. The stability of these poses was evaluated using PoseScore, which was based on the observed RMSD (relative to the initial ligand coordinates) and the persistence of hydrogen bonds during the metadynamics simulations, quantified by PersScore. A linear combination of PoseScore and PersScore were calculated for understanding the strength of binding of microbial lactones with PL. Where,

$$\mathrm{CompScore} = \mathrm{PoseScore} - 5\ \mathrm{X}\ \mathrm{PersScore}$$

2.7 Water Transport Pathway Analysis

For analysing the water transport pathway in the PL enzyme structure, tunnel identification was performed using CAVER 3.0, integrated with PyMOL 2.3.0.[34,43] The cluster zero of PL apo structure after 100 ns MD was taken as the input PDB for the calculation. To approximate the individual atoms in the structure, the number of balls was specified to 12, with a van der Waals (VDW) radius equal to that of the smallest atom in the structure (H atom). This will allow the granularity of atom approximation, thereby impacting the accuracy of the Voronoi diagram. To ensure the important tunnel branches in the structure, a shell radius of 5 Å, which was larger than the bottleneck radius of the tunnels and a shell depth of 7 Å, indicating maximal depth of surface regions below the bulk solvent, were considered. This will identify tunnels without overestimating tunnel slithering on the protein surface. In order to nullify irrelevant tunnels a minimum probe radius cut off was set to 2.8 Å. The clustering threshold by which the tree hierarchy of tunnels get clustered, was set to 3.5. The calculation was started by defining the initial starting point as S153, as it is the crucial catalytic residue of PL. The maximal distance from the initial starting point to the calculation starting point was set to the default value of 3 Å.[43] Additionally, the desired radius, indicating the minimum distance between the starting Voronoi vertex and the atoms representing the input structure of PL, was set to the default value of 5 Å.[43] The lowest cost tunnel, representing the identified pathways in PL structure was analysed for its water and inhibitor entry and exit in the structure.

3. Results And Discussion

3.1. Factors Influencing Microbial Lactone Binding to Pancreatic Lipase: Contribution of Non-Covalent Interactions

Figure 1 illustrates the dynamics and stability of non-covalent binding of microbial lactone and synthetic lactone inhibitors of PL as observed in the 100 ns molecular dynamics simulation. It also accounts the conformational variations of the inhibitors and the adaptation of PL active site during the inhibitor binding. During the simulations, all the lactone inhibitors preferred to bind at the catalytic site (S1-S2) of PL open conformation. This is crucial because inhibiting the enzyme's catalytic site can mitigate its hyperactivity in the context of hyperlipidaemia by preventing the access with dietary lipids.[44,45] The non-covalent binding poses of lactone inhibitors with PL active site, indicating their alkyl chain resting at S1-S3 channel (β-5 and lid) and S2 sub-pocket (β-9 loop), amide branch near to the gate keeper residues D80 and R257, and β-lactone ring at the vicinity of catalytic S153 (Figure S2 to S4). During the 100 ns MD, as indicated in Fig. 1A-C, PL-lactone complexes showed minimal deviation of protein backbone (Cα) with RMSD ranging from 0.4 to 2.58 Å. Among the microbial lactones Panclicin C and ebelectone A were showing comparatively higher fluctuation in the active site. The lower RMSD of the binding site residues with respect to the lactone inhibitors-binding indicated minimal perturbation of binding poses contributing to their stability in the pocket.

As illustrated in Fig. 1D-F, the apo form of PL exhibits flexibility in the β9 loop (205–223) and at the colipase region. Upon binding of lactone inhibitors, such as Orlistat, Valilactone, Esterastin, Panclicin B-D, ebelectone B, and Cetilistat, at the active site, there was an increased fluctuation in the S1 (β5 loop), S2 (β9 loop), and S3 (lid) sub-pockets. Conversely, the fluctuations at colipase region were significantly reduced. The synthetic lactone inhibitors of PL, Orlistat and Cetilistat, exhibit binding pose stability comparable to that of microbial lactones within the active site, demonstrating their effective binding and similar impact on enzyme conformation. These observations suggest that lactone inhibitors induce notable conformational changes in the flexible regions of the PL enzyme, which also stabilizes the colipase region compare to the apo structure and potentially resulting in a more stable inhibitor-bound PL complex.

The alterations in the β9 loop, lid, and colipase regions of the PL enzyme play a crucial role in its interaction with lipid substrates.[6] The observed changes reflect the enzyme's adaptive nature and its interaction with microbial lactones inhibitors. During the 100 ns MD simulation, all lactones formed an average of 8–12 hydrogen bonds with the active site residues of PL, including the crucial residues G76 and F78 in the oxyanion hole, H152, S153, and H264 at the catalytic site and D80 and R257 at the entry gate and. Notably, more structurally diverse lactones, such as Esterastin, Valilactone, Orlistat, Lipstatin, and Panclicins established more than 10 hydrogen bonds with these active site residues. This is majorly contributed by their potential functional groups, β-lactone and amide branch compare to the Ebelactones

and Cetilistat (Scheme 1). The presence and persistence of hydrogen bonds, particularly with oxyanion hole residues in the S1 sub-pocket and with catalytic S153, play a significant role in stabilizing the inhibitor's binding pose. Unlike this, the position of β-lactone ring of Valilactone, Ebelactone B and Cetilistat were unfavourably away from the catalytic S153, accounting to their smaller number of interaction and hydrogen bonds during the simulation (Figure S2 to S4).

The structural features of microbial lactones, such as the β-lactone ring, amide branch, and alkyl chains, have a significant impact on their total binding energy. These features contribute to the active site occupancy, influencing the overall binding affinity of the lactones. The binding free energy (ΔG_{MMGBSA}, Amber ff14SB force field) of lactone inhibitors in PL active site pocket depicted in Figure S5. It is vivid that the microbial lactones and Orlistat which are structurally rich with the key functional groups, discussed earlier, showed the highest binding free energy. Whereas Ebelactone A, ebelectone B along with Cetilistat showed comparatively less binding free energy. The major contributing factors for this variation are electrostatic (EEL), van der Waals (VDWAALS), and non-polar solvation energy (ESURF) with the active site residues as well as solvent in the system Fig. 2 and Figure S5). Among the group, Esterastin exhibited the superior binding energy, -55.52 kcal/mol, followed by Orlistat, -48.22 kcal/mol. This substantial binding energy

is primarily due to their significant electrostatic interactions, predominantly arising from the β-lactone ring interacting with residues F78, H152, S153, F216, A260, and H264. The amide branch lies at the S1 sub-pocket, contributing to this coulombic energy through hydrogen bonds with the loop.

Additionally, van der Waals interactions also contributed significantly, especially from the alkyl chain interacting with residues I79, D80, Y115, S153, P181, F216, A261, L265, and Y268. These interactions are detailed in the per-residue decomposition analysis (Fig. 2C). The same trend can be seen in Lipstatin, and Panclicins. In the case of Valilactone the position of β-lactone, away from S153 have tremendously reduced the electrostatic energy as indicated in Fig. 2 (Figure S2B and Figure S5). Among the Panclicins, Panclicin C showed binding energy comparable to Orlistat, with − 47.58 kcal/mol, also it is the potent PL inhibitor reported earlier (IC_{50}, 0.62 μM) in the group.[15] The non-covalent binding free energy was further assessed using the OPLS3e force field in Maestro. Except for Esterastin, Panclicin C, and Cetilistat, the binding energies of the other compounds were found to be increased (Fig. 6A). Despite this, Ebelactone B and Cetilistat remained the least bound compounds, as indicated by their binding energy from the investigation.

The structural advantages of Esterastin like microbial lactones and Orlistat over Ebelactones and Cetilistat have reflected in their superior binding affinity and stability within the PL enzyme's active site. The positioning of β-lactone rings near the oxyanion hole and S153 increases the likelihood of forming a covalent bond with catalytic S153. This is similar to how tetrahydroLipstatin (Orlistat) binds PL, where the β-lactone ring forms a covalent bond with the nucleophilic serine residue, enhancing its inhibitory effect.[13,14]

3.2. Insights Into Covalent Binding Dynamics of Microbial Lactones with Pancreatic Lipase

Figures 3–5 illustrate the CovDock-simulated covalent binding poses of 12 lactone inhibitors of PL, minimized in the gas phase using OPLS3e force field of Maestro. As illustrated, the lactone warhead, β-lactone covalently binds to the nucleophilic S153 after the ring opening, distinguishing it from non-covalent binding. Except Lipstatin and Cetilistat the ester bonds of all other lactones possessed hydrogen bond with G76 of oxyanion hole and catalytic H264 (Fig. 3–5). This is important as oxyanion hole in the PL is known to stabilise the ester bond by neutralising the negative charge on it, which is further enhanced by the presence of catalytic H264 in the vicinity.[7] Except for Valilactone, Ebelactone B, and Cetilistat, the covalent binding poses of the lactones, closely resembled their non-covalent binding poses (Fig. 3–5 and Figure S2-S5). This similarity was indicated by the positions of the alkyl chains, with one at the S2 sub-pocket and the other at the S1-S3 channel, providing stability through interactions with hydrophobic residues. Additionally, the amide branch was stabilized by hydrogen bonds with residues D80 and R257. In the case of Ebelactone B and Cetilistat, due to the ester bond formation with S153, the alkyl chains were drawn in between S1-S3 channel by means of hydrophobic interactions with the residues F78, I79, A260, S261, L265 (Fig. 5). Upon the ester bond formation, Valilactone followed the trend of Orlistat and similar lactones by increasing its number of interactions with PL's catalytic residues and oxyanion hole.

This overall binding poses arrangements upon the covalent bond formation have influenced profoundly to their binding energy (ΔG_{MMGBSA}, OPLS3e force field), as indicated in Fig. 6B. Compare to the non-covalent binding energy the binding energy of covalently bound lactones were significantly improved, except for Orlistat. This has arisen from the increased van der Waals interaction and decreased desolvation energy in the covalently bound complex.

Evidently, Valilactone, Esterastin, Lipstatin, Panclicin A, Panclicin C, Panclicin D, Panclicin E, and Ebelactone B, covalent bonding caused one of their alkyl chains to extend towards the S2 hydrophobic pocket. This has resulted in increased van der Waals interactions and consequently a higher ΔG_{vdW}. Also, the tighter covalent ester bond of lactones with PL have resulted in a low desolvation energy (ΔG_{solv}) compare to the non-covalent binding (Fig. 6). Typically, when a ligand binds tightly to a protein, its desolvation energy decreases significantly, due to the removal of solvent molecules that were originally surrounding the ligand. This trend was observed in the 100 ns MD trajectory analysis of non-covalent and covalently bound lactone–PL complexes, with the exception of Panclicin E, Ebelactone A, and Cetilistat, as illustrated in Fig. 8C. The decrease in desolvation energy is typically a favourable factor, as it contributes to a more negative binding free energy, making the binding process thermodynamically more favourable.

Figure 7 illustrates the binding pose metadynamics - stability and strength of covalent binding of microbial lactones with PL enzyme. Upon sampling various binding poses using BPMD the low-energy

binding modes were represented in the Fig. 3–5. During the 100 ns metadynamics simulation PL-lactone complexes displayed minimal deviations in the protein backbone (Cα), with RMSD values less than 2.5 Å, suggesting minimal perturbations in binding poses. In contrast to the non-covalent binding, covalent binding of Orlistat, Esterastin, Panclicin C, Ebelactones and Cetilistat have triggered residual fluctuation more at S1 and S3 sub-pockets, especially at T70, I73, K296 and C297. While, fluctuations in the colipase region were notably minimal. This has suggested that covalent binding of lactone inhibitors induce significant conformational changes at the S1 and S3 sub pockets possibly due to the conformational arrangement of alkyl chain and amide branch, to establish an effective binding at the active site pocket. Upon binding of the inhibitors, the binding sub-pockets of PL—S1, S2, and S3, were observed to be flexible, as reported previously in our earlier studies.[45,46] Such changes potentially lead to a more stable inhibitor-bound PL complex.[45,46] The flexibility observed in the S1 and lid regions are crucial for enzyme interaction with lipid substrates, highlighting the enzyme's adaptability and its interaction with microbial lactone inhibitors.

The persistence or stability of the covalently bound lactone inhibitors was reflected by PersScore values greater than 0.6 for Esterastin, Lipstatin, Orlistat, Panclicin A, Panclicin B, Panclicin D, Panclicin E, and Ebelactone B (Fig. 7G). A PersScore above 0.6 indicates that these ligands maintain stable interactions and binding modes during the simulation, suggesting robust and reliable binding poses. This observation aligns with the analysis of key interactions, such as hydrogen bonds and hydrophobic contacts, observed with PL during metadynamics trajectory visualization using VMD. The stability of these inhibitors, binding covalently to PL, was further corroborated by PoseScore values less than 2.5, except for Orlistat and Cetilistat, which were had a PoseScore of morethan 3 (Fig. 7). Further analysis of the directional relationship between the stability of inhibitors (PoseScore) and their reported *in vitro* PL inhibition values ($_{P}IC_{50}$, the negative log of IC_{50}), revealed an important correlation (Fig. 7I). Inhibitors that demonstrate greater stability at the PL catalytic site, particularly those forming covalent bonds, tend to exhibit higher PL inhibition capacities. Among the microbial lactones studied, Valilactone showed the lowest PoseScore value of 1.6, indicating exceptional stability. This stability corresponds to its reported high potency, with an IC_{50} value of 0.00035 μM, making Valilactone the most potent microbial lactone inhibitor reported to date.[10] The combination of PersScore and PoseScore values, as indicated by the CompScore, further confirmed that, Cetilistat bound weakly at the PL active site (Fig. 7H).

3.3. Exploring Reversible Covalent Inhibition of Microbial Lactones Towards Pancreatic Lipase

The analysis of water tunnel pathways and the number of water molecules within the structure of PL provides significant insights into water transit mechanisms and its role in PL-inhibitor interactions. In aqueous solution, the inhibition of lipase by Orlistat exhibits reversible characteristics, underscoring the importance of water in its reversible covalent inhibition of PL.[14] Since water acts as the final proton donor in the hydrolysis reaction, monitoring water tunnels is crucial for investigating the potential entry of water molecules near the catalytic residue S153.[7] This is important for understanding how water

might facilitate covalent bond cleavage in an aqueous environment, especially in the context of how inhibitors like Orlistat or microbial lactones may affect the PL activity during the overdose or long-term use. The probe radius of 0.9 Å and shell radius 5 Å in Caver tunnel analysis identifies the narrowest pathways that can still accommodate water molecules (with a van der Waals radius of 1.4 Å), considering tunnel flexibility and varying diameters, as illustrated in Fig. 8A. While these tunnels allow water passage, they may also restrict inhibitors with larger van der Waals radii.

The major tunnels present in the PL active site are illustrated in Fig. 8A. Among the several identified tunnels, those with a water throughput or transit probability greater than 0.5 (50%) were prioritized to identify the top five potent pathways in the system Fig. 8B. Considering the bottleneck radius, length, curvature and the throughput values tunnels at S2-S3 (yellow) channel and S2 sub-pocket (green) were considered as the favourable routes of water transit pathways at the PL active site. Whereas the two tunnels (red and blue) at S1-S3 channel can potentially accommodate other ions larger than water.

Further analysis of the molecular dynamics (MD) and metadynamics trajectories estimated that the average number of water molecules at the catalytic site near S153 ranged from 4 to 11 in the cases of non-covalent binding, and from 0 to 13 in cases of covalent inhibition (Fig. 8C). Except for Panclicin C, Panclicin E, Ebelactone A, and Cetilistat, the number of water molecules decreased upon covalent bond formation with other lactones, reflected in reduced desolvation and suggesting increased binding stability in the pocket. Nevertheless, the presence of water molecules near S153 in the context of microbial lactone binding may facilitate the hydrolysis of their covalent bonds, potentially reverting the PL enzyme to its active form. This highlights the potential of reversible covalent inhibition by microbial lactones as a strategy for obesity management.

These insights suggest that microbial lactones, containing the warhead – β-lactone can potentially reduce PL activity through their covalent inhibition mechanisms, offer a promising pharmacological strategy for developing anti-obesity therapeutics. The potential of these compounds to selectively and effectively inhibit PL paves the way for future research and development of targeted obesity treatments, harnessing the natural bioactivity of microbial lactones.

4. Conclusion

The present study provides molecular-level insights into the binding stability and inhibition mechanisms of microbial and synthetic lactone-based pancreatic lipase inhibitors. Molecular dynamics simulations showed that several beta-lactone-containing inhibitors, particularly esterastin, valilactone, orlistat, and selected panclicins, maintained stable binding poses within the S1-S2 catalytic region of the open PL conformation. Their stability was supported by persistent interactions with active-site residues, including the oxyanion-hole residues and catalytic Ser153, as well as by favorable hydrophobic contacts involving the alkyl chains.

Covalent docking and binding-pose metadynamics further suggested that beta-lactone-containing inhibitors can adopt stable covalent binding orientations with catalytic Ser153. Compared with non-

covalent complexes, the modeled covalent complexes showed improved binding energetics, mainly through increased van der Waals interactions and reduced desolvation energy. Esterastin showed favorable covalent binding energy, whereas valilactone displayed a strong binding-pose stability score, consistent with the importance of beta-lactone positioning, alkyl-chain orientation, and active-site complementarity in PL inhibition.

Water tunnel analysis provided additional insight into the possible role of local hydration near Ser153. The presence and accessibility of water molecules around the catalytic region may influence hydrolytic accessibility and the potential reversibility of lactone-mediated covalent inhibition. Together, these findings suggest that microbial lactones provide useful structural scaffolds for the rational design of pancreatic lipase inhibitors. The study highlights how non-covalent recognition, covalent adduct stability, binding energetics, and water hydration in active site collectively contribute to lactone-based PL inhibition.

Declarations

Supporting Information: The binding poses and binding energies of a covalent inhibitors of PL are depicted in Figures S1-S5 in the supplementary information.

CRediT authorship contribution statement

Sanjay Kottekad conducted the investigation, curated and analyzed the data, and wrote the manuscript. Dandamudi Usharani conceptualized the project, provided resources and supervision, data analysis, and manuscript writing.

AI tool: The authors used ChatGPT (OpenAI, GPT-5.0) to assist with grammar check, language refinement for clarity and graphical abstract illustration to the manuscript. The authors critically reviewed, verified, and edited all AI-assisted content and take full responsibility for the accuracy, integrity, and final content of the manuscript.

Declaration of competing interest

The authors declare no competing financial interest that could have appeared to influence the work reported in this paper.

Funding Sources

This work was supported by Anusandhan National Research Foundation (ANRF) SERB – POWER GRANT (File No: SPG/2021/002205).

ACKNOWLEDGEMENTS

SK thanks Department of Biotechnology (DBT), India (File No.: BT/PR10329/PFN/20/776/2013) and Council of Scientific and Industrial Research (CSIR), New Delhi (File No.: 31/0005(12326)/2021-EMR-

I)for the research fellowships. DU thanks ANRF-SERB – POWER GRANT (File No: SPG/2021/002205) for research grant that provided computing facilities. We thank Dr. Sudarshan of Schrodinger for his inputs.

References

1. Egloff MP, Marguet F, Buono G, Verger R, Cambillau C, van Tilbeurgh H (1995) The 2.46 Å Resolution Structure of the Pancreatic Lipase-Colipase Complex Inhibited by a C11 Alkyl Phosphonate. Biochem 34:2751–2762
2. Akoh CC, Lee GC, Liaw YC, Huang TH, Shaw JF (2004) GDSL Family of Serine Esterases/Lipases. Prog Lipid Res 43(6):534–552
3. Gadde KM, Martin CK, Berthoud HR, Heymsfield SB, Obesity (2018) Pathophysiology and Management. J Am Coll Cardiol 71(1):69–84
4. Lin X, Li H, Obesity (2021) Epidemiology, Pathophysiology, and Therapeutics. Front Endocrinol 12:706978
5. Wright SM, Aronne LJ (2012) Causes of Obesity. Abdom Radiol 37(5):730–732
6. Lowe ME (2002) The Triglyceride Lipases of the Pancreas. J Lipid Res 43:2007–2016
7. Van Tilbeurgh H, Egloff MP, Martinez C, Rugani N, Verger R, Cambillau C (1993) Interfacial Activation of the Lipase–Procolipase Complex by Mixed Micelles Revealed by X-Ray Crystallography. Nature 362(6423):814–820
8. Borgström B (1988) Mode of Action of TetrahydroLipstatin: A Derivative of the Naturally Occurring Lipase Inhibitor Lipstatin. Biochim. Biophys Acta (BBA)-Lipids Lipid Metab 962(3):308–316
9. Hadvary P, Sidler W, Meister W, Vetter W, Wolfer H (1991) The Lipase Inhibitor Tetrahydropstatin Binds Covalently to the Putative Active Site Serine of Pancreatic Lipase. J Biol Chem 266(4):2021–2027
10. Umezawa H, Aoyagi T, Hazato T, Uotani K, Kojima F, Hamada M, Takeuchi T (1978) Esterastin, an Inhibitor of Esterase, Produced by Actinomycetes. J Antibiot 31(6):639–641
11. Umezawa H, Aoyagi T, Uotani K, Hamada M, Takeuchi T, Takahashi S (1980) Ebelactone, an Inhibitor of Esterase, Produced by Actinomycetes. J Antibiot 33(12):1594–1596
12. Kitahara M, Asano M, Naganawa H, Maeda K, Hamada M, Aoyagi T, Umezawa H, Iitaka Y, Nakamura H (1987) Valilactone, an Inhibitor of Esterase, Produced by Actinomycetes. J Antibiot 40(11):1647–1650
13. Weibel EK, Hadvary P, Hochuli E, Kupfer E, Lengsfeld H (1987) Lipstatin, an Inhibitor of Pancreatic Lipase, Produced by Streptomyces toxytricini I. Producing Organism, Fermentation, Isolation and Biological Activity. J Antibiot 40(8):1081–1085
14. Lupianez-Merly C, Dilmaghani S, Vosoughi K, Camilleri M (2024) Pharmacologic Management of Obesity-Updates on Approved Medications, Indications, and Risks. Alim Pharmacol Ther 59(4):475–491

15. Yamada Y, Kato T, Ogino H, Ashina S, Kato K (2008) Cetilistat (ATL-962), a Novel Pancreatic Lipase Inhibitor, Ameliorates Body Weight Gain and Improves Lipid Profiles in Rats. Horm Metab Res 40(08):539–543
16. Mutoh M, Nakada N, Matsukuma S, Ohshima S, Yoshinari K, Watanabe J, Arisawa M (1994) Panclicins, Novel Pancreatic Lipase Inhibitors I. Taxonomy, Fermentation, Isolation and Biological Activity. J Antibiot 47(12):1369–1375
17. Liu DZ, Wang F, Liao TG, Tang JG, Steglich W, Zhu HJ, Liu JK (2006) Vibralactone: A Lipase Inhibitor with an Unusual Fused β-Lactone Produced by Cultures of the Basidiomycete Boreostereum vibrans. Org Lett 8(25):5749–5752
18. Berman HM, Westbrook J, Feng Z, Gilliland G, Bhat TN, Weissig H, Shindyalov IN, Bourne PE (2000) The Protein Data Bank. Nucleic Acids Res 28:235–242
19. PDB DOI https://doi.org/10.2210/pdb1LPB/pdb
20. Egloff MP, Marguet F, Buono G, Verger R, Cambillau C, van Tilbeurgh H (1995) The 2.46 Å Resolution Structure of the Pancreatic Lipase-Colipase Complex Inhibited by a C11 Alkyl Phosphonate. Biochem 34:2751–2762
21. Bas DC, Rogers DM (2007) PROPKA: VERSION 2.0. Iowa City/Copenhagen
22. Humphrey W, Dalke A, Schulten K (1996) VMD - Visual Molecular Dynamics. J Mol Graphics 14:33–38
23. Case DA, Belfon K, Ben-Shalom IY, Brozell SR, Cerutti DS, Cheatham TE, Cruzeiro III, Darden VWD, Duke TA, Giambasu RE, Gilson G, Gohlke MK, Goetz H, Harris AW, Izadi R, Izmailov S, Kasavajhala SA, Kovalenko K, Krasny A, Kurtzman R, Lee T, LeGrand TS, Li S, Lin P, Liu C, Luchko J, Machado T, Man M, Merz V, Miao KM, Mikhailovskii Z, Monard O, Nguyen G, Onufriev H, Pan A, Pantano F, Qi S, Rahnamoun R, Roe A, Roitberg DR, Sagui A, Schott-Verdugo C, Shajan S, Shen A, Simmerling J, Skrynnikov CL, Smith NR, Swails J, Walker J, Wang RC, Wang J, Wei J, Wolf H, Wu RM, Xue X, York Y, Zhao S Kollman, P. A. AMBER 2020 and AmberTools 2020; University of California, San Francisco.
24. Kim S, Chen J, Cheng T, Gindulyte A, He J, He S, Li Q, Shoemaker BA, Thiessen PA, Yu B, Zaslavsky L, Zhang J, Bolton EE (2023) PubChem 2023 Update. Nucleic Acids Res 51(D1):D1373–D1380
25. Frisch MJ, Trucks GW, Schlegel HB, Scuseria GE, Robb MA, Cheeseman JR, Scalmani G, Barone V, Petersson GA, Nakatsuji H, Li X, Caricato M, Marenich AV, Bloino J, Janesko BG, Gomperts R, Mennucci B, Hratchian HP, Ortiz JV, Izmaylov AF, Sonnenberg JL, Williams-Young D, Ding F, Lipparini F, Egidi F, Goings J, Peng B, Petrone A, Henderson T, Ranasinghe D, Zakrzewski VG, Gao J, Rega N, Zheng G, Liang W, Hada M, Ehara M, Toyota K, Fukuda R, Hasegawa J, Ishida M, Nakajima T, Honda Y, Kitao O, Nakai H, Vreven T, Throssell K, Montgomery JA, Peralta JE, Ogliaro J, Bearpark F, Heyd MJ, Brothers JJ, Kudin EN, Staroverov KN, Keith VN, Kobayashi TA, Normand R, Raghavachari J, Rendell K, Burant AP, Iyengar JC, Tomasi SS, Cossi J, Millam M, Klene JM, Adamo M, Cammi C, Ochterski R, Martin JW, Morokuma RL, Farkas K O.; Foresman, J. B.; Fox, D. J. Gaussian 16, Revision A.03; Gaussian, Inc.: Wallingford, CT, 2016.

26. Pettersen EF, Goddard TD, Huang CC, Couch GS, Greenblatt DM, Meng EC, Ferrin TE (2004) UCSF Chimera—A Visualization System for Exploratory Research and Analysis. J Comput Chem 25(13):1605–1612
27. Trott O, Olson AJ (2010) AutoDock Vina: Improving the Speed and Accuracy of Docking with a New Scoring Function, Efficient Optimization, and Multithreading. J Comput Chem 31(2):455–461
28. Alexander ST (1986) The Method of Steepest Descent. Adapt Signal Process. 46–67
29. Navon IM, Legler DM (1987) Conjugate-Gradient Methods for Large-Scale Minimization in Meteorology. Mon Weather Rev 115:1479–1502
30. Izaguirre JA, Catarello DP, Wozniak JM, Skeel RD (2001) Langevin Stabilization of Molecular Dynamics. J Chem Phys 114(5):2090–2098
31. Berendsen HJC, Postma JPM, Van Gunsteren WF, Dinola A, Haak JR (1984) Molecular Dynamics with Coupling to an External Bath. J Chem Phys 81(8):3684–3690
32. Elber R, Ruymgaart AP, Hess BSHAKE, Parallelization (2011) Eur Phys J Spec Top 200(1):211–223
33. Darden T, York D, Pedersen L (1993) Particle Mesh Ewald: An N·log(N) Method for Ewald Sums in Large Systems. J Chem Phys 98(12):10089–10092
34. The PyMOL Molecular Graphics System, Version 1.7, Schrödinger, LLC
35. GraphPad, Prism Version 10, GraphPad Software, San Diego, CA
36. Schroder J, Klinger A, Oellien F, Marhofer RJ, Duszenko M, Selzer PM (2013) Docking-Based Virtual Screening of Covalently Binding Ligands: An Orthogonal Lead Discovery Approach. J Med Chem 56:1478–1490
37. Maestro v9.5 (2020) Schrodinger, Inc.: Portland
38. Friesner RA, Banks JL, Murphy RB, Halgren TA, Klicic JJ, Mainz DT, Repasky MP, Knoll EH, Shelley M, Perry JK, Shaw DE, Francis P, Shenkin PS (2004) Glide: A New Approach for Rapid, Accurate Docking and Scoring. 1. Method and Assessment of Docking Accuracy. J Med Chem 47:1739–1749
39. Li J, Abel R, Zhu K, Cao Y, Zhao S, Friesner RA (2011) The VSGB 2.0 Model: A Next Generation Energy Model for High Resolution Protein Structure Modeling. Proteins 79:2794–2812
40. Fusani L, Palmer DS, Somers DO, Wall ID (2020) Exploring Ligand Stability in Protein Crystal Structures Using Binding Pose Metadynamics. J Chem Inf Model 60(3):1528–1539
41. Lukauskis D, Samways ML, Aureli S, Cossins BP, Taylor RD, Gervasio FL (2022) Open Binding Pose Metadynamics: An Effective Approach for the Ranking of Protein–Ligand Binding Poses. J Chem Inf Model 62(23):6209–6216
42. Clark AJ, Tiwary P, Borrelli K, Feng S, Miller EB, Abel R, Friesner RA, Berne BJ (2016) Prediction of Protein-Ligand Binding Poses via a Combination of Induced Fit Docking and Metadynamics Simulations. J Chem Theory Comput 12(6):2990–2998
43. Chovancova E, Pavelka A, Benes P, Strnad O, Brezovsky J, Kozlikova B, Gora A et al (2012) CAVER 3.0: a tool for the analysis of transport pathways in dynamic protein structures. : e1002708

44. Yun JW (2010) Possible Anti-Obesity Therapeutics from Nature—A Review. Phytochemistry 71(14–15):1625–1641

45. Kottekad S, Usharani D (2025) Phytochemical Analysis of Triphala Extract, In Vitro and In Silico Evaluation of Pancreatic Lipase Inhibition for Obesity Management. Plant Foods Hum Nut 80(1):65

46. Kottekad S, Roy S, Usharani DA (2024) Computational Study to Probe the Binding Aspects of Potent Polyphenolic Inhibitors of Pancreatic Lipase. J Biomol Struct Dyn 42(7):3472–3491

Figures

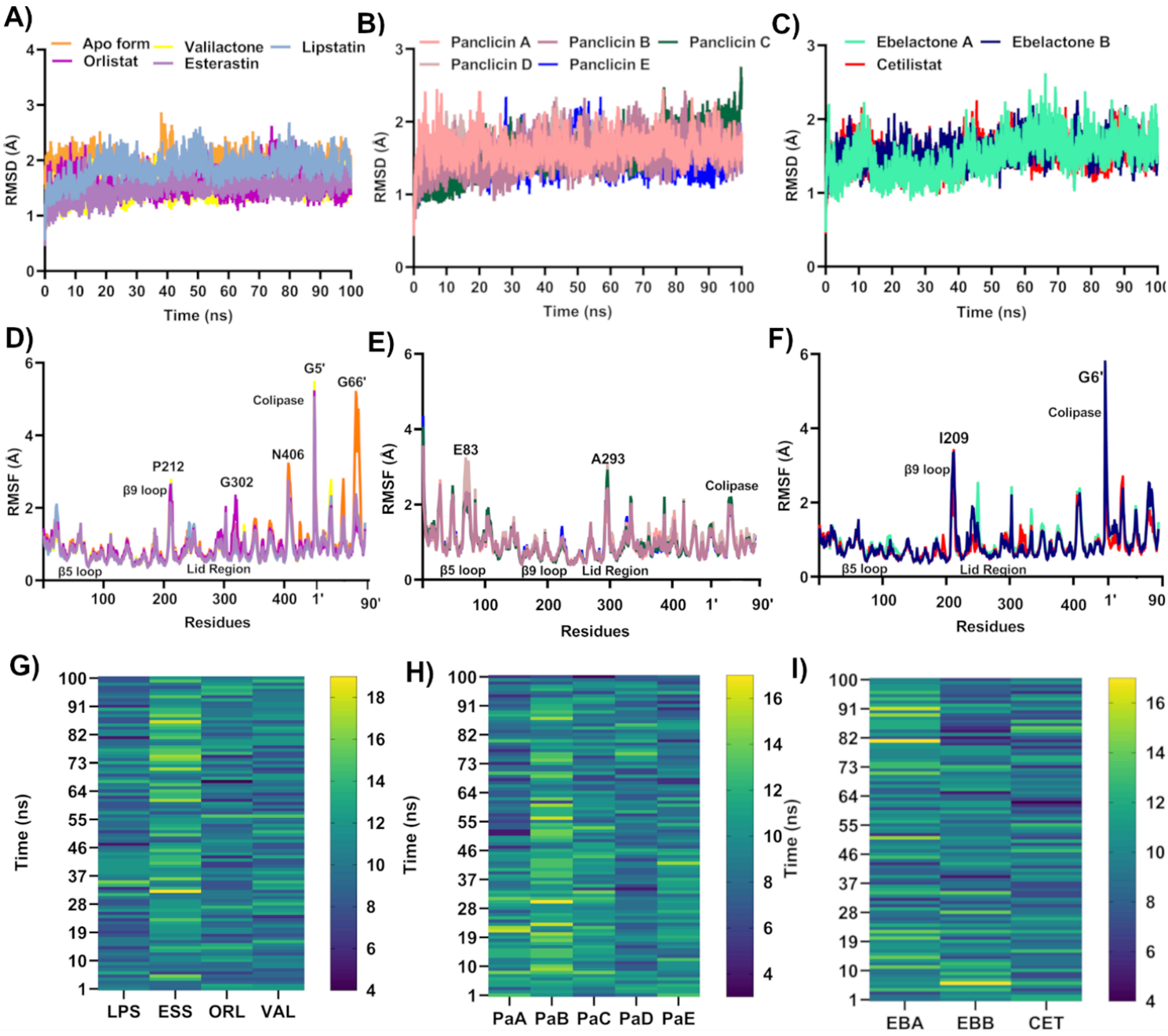


Figure 1

Figure A to C - Root Mean Square Deviation-RMSD, D to E - Root Mean Square Fluctuation-RMSF analyses of apo form of pancreatic lipase (PL) and its complexes with various microbial lactones, including Esteradtin, Valilactone, Lipstatin, Orlistat, Panclicin A-E, Ebelectone A and B, and Cetilistat, in different colour codes. The heat map from G to I shows the number of hydrogen bond interactions of these lactone inhibitors throughout the 100 ns Molecular Dynamics (MD) simulations.

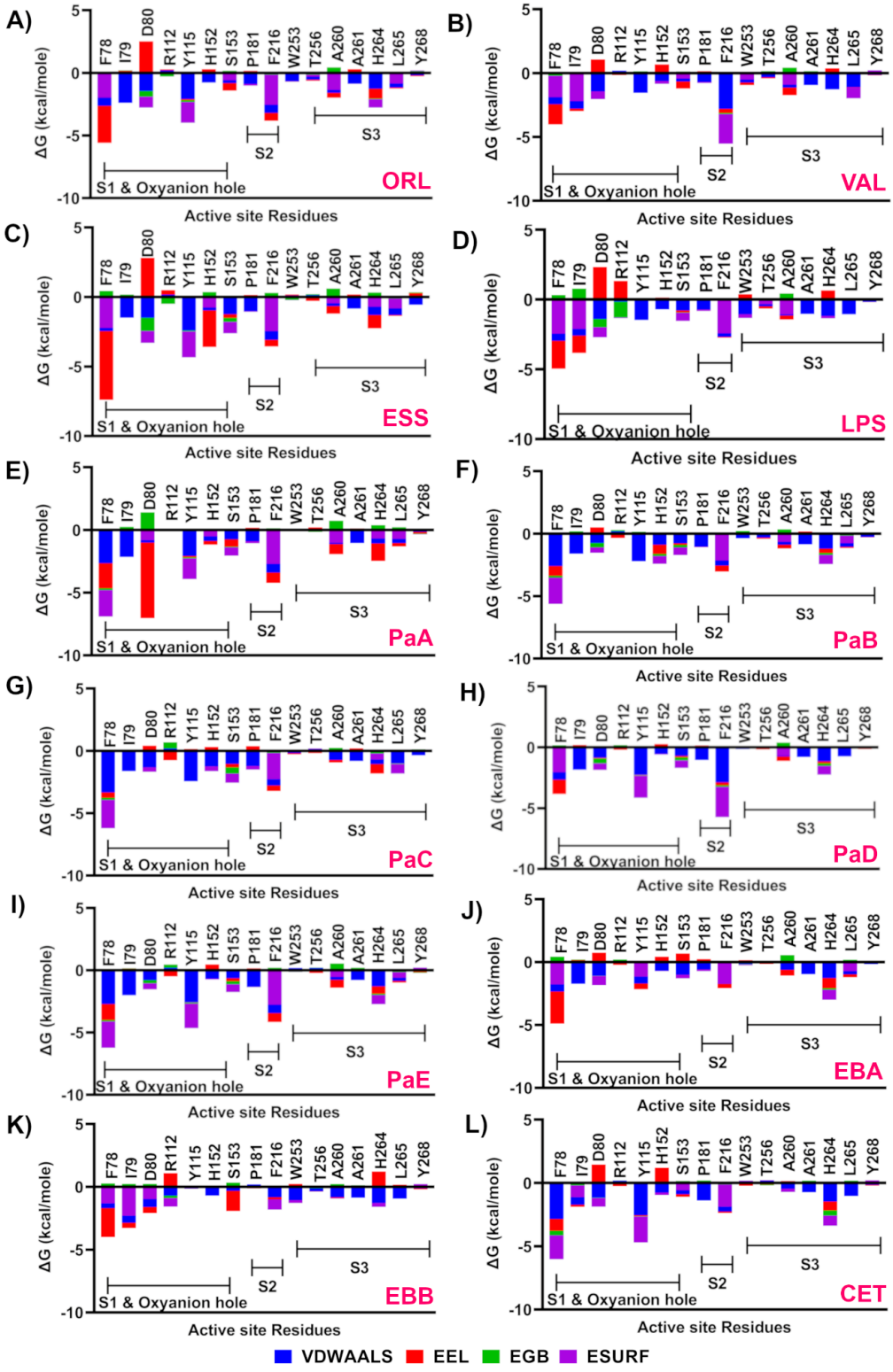


Figure 2

The figure A to L illustrates per residue decomposition analysis of non-covalent binding energy ($\Delta G_{(MMGBSA)}$ in kcal/mol) calculated in AMBER forcefield. Residual contribution of binding energy, including electrostatic (EEL), van der Waals (VDWAALS), electrostatic contribution to the solvation free energy calculated GB (EGB), electrostatic contribution related to the solvent-accessible surface area of the inhibitor (ESURF), of lactone inhibitors of pancreatic lipase, ORL-Orlistat, VAL-Valilactone, ESS-Esterastin, LPS-Lipstatin, PaA-Panclicin A, PaB-Panclicin B, PaC-Panclicin C, PaD-Panclicin D, PaE-Panclicin E, EBA-Ebelactone A, EBB-Ebelactone B and CET-Cetilistat.

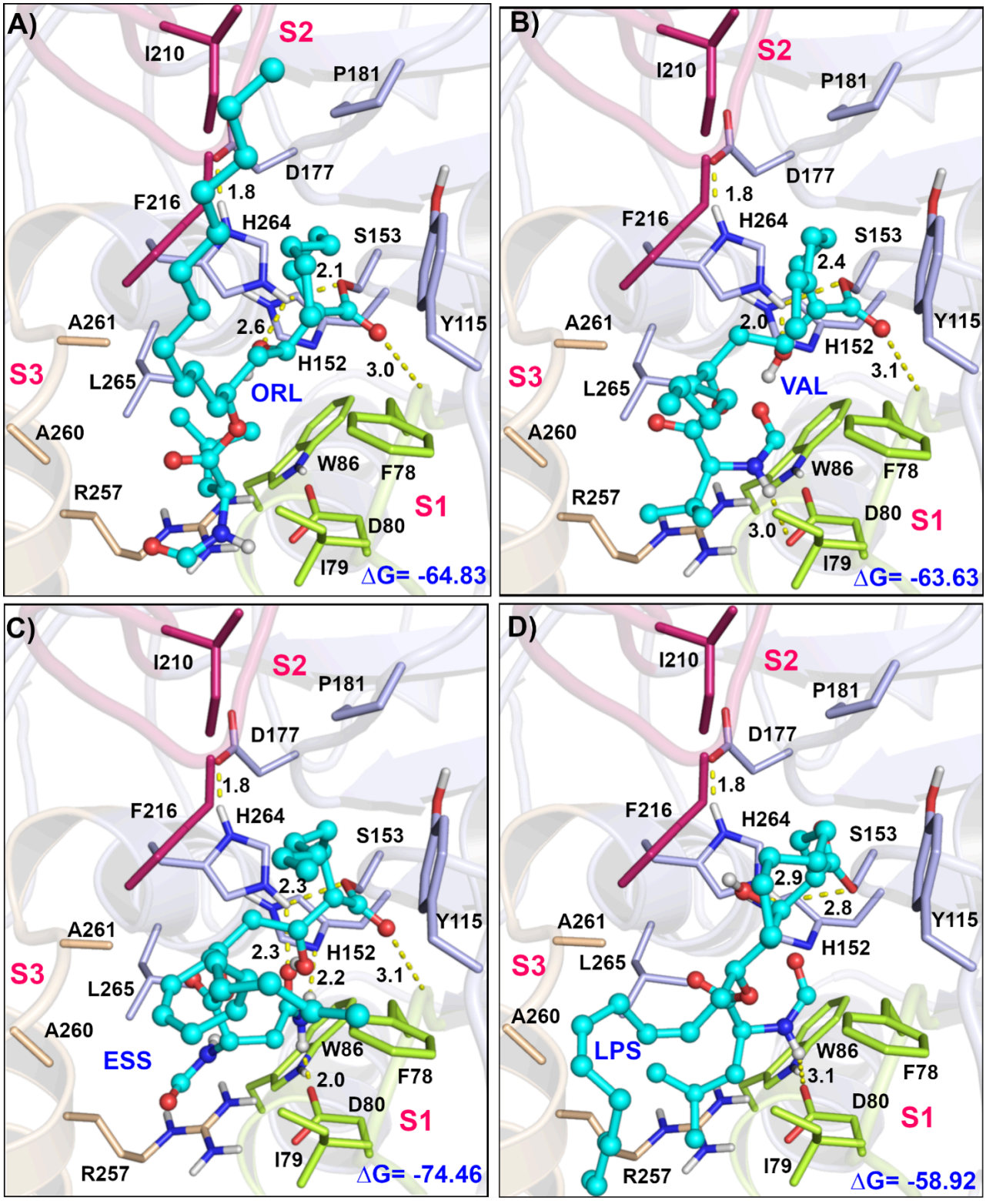


Figure 3

Covalent binding poses of ORL-Orlistat (A), VAL-Valilactone (B), ESS-Esterastin (C) and LPS-Lipstatin (D) in the active site pocket of pancreatic lipase (PL) after a 100 ns metadynamics simulation run. Interacting residues of the pancreatic lipase protein are shown in limon, representing β-5 loop and S1 sub-pocket, warm pink, representing β-9 loop and S2 sub-pocket, in wheat colour, representing lid region or S3 sub pocket. Hydrogen bonding interactions are illustrated with yellow lines.

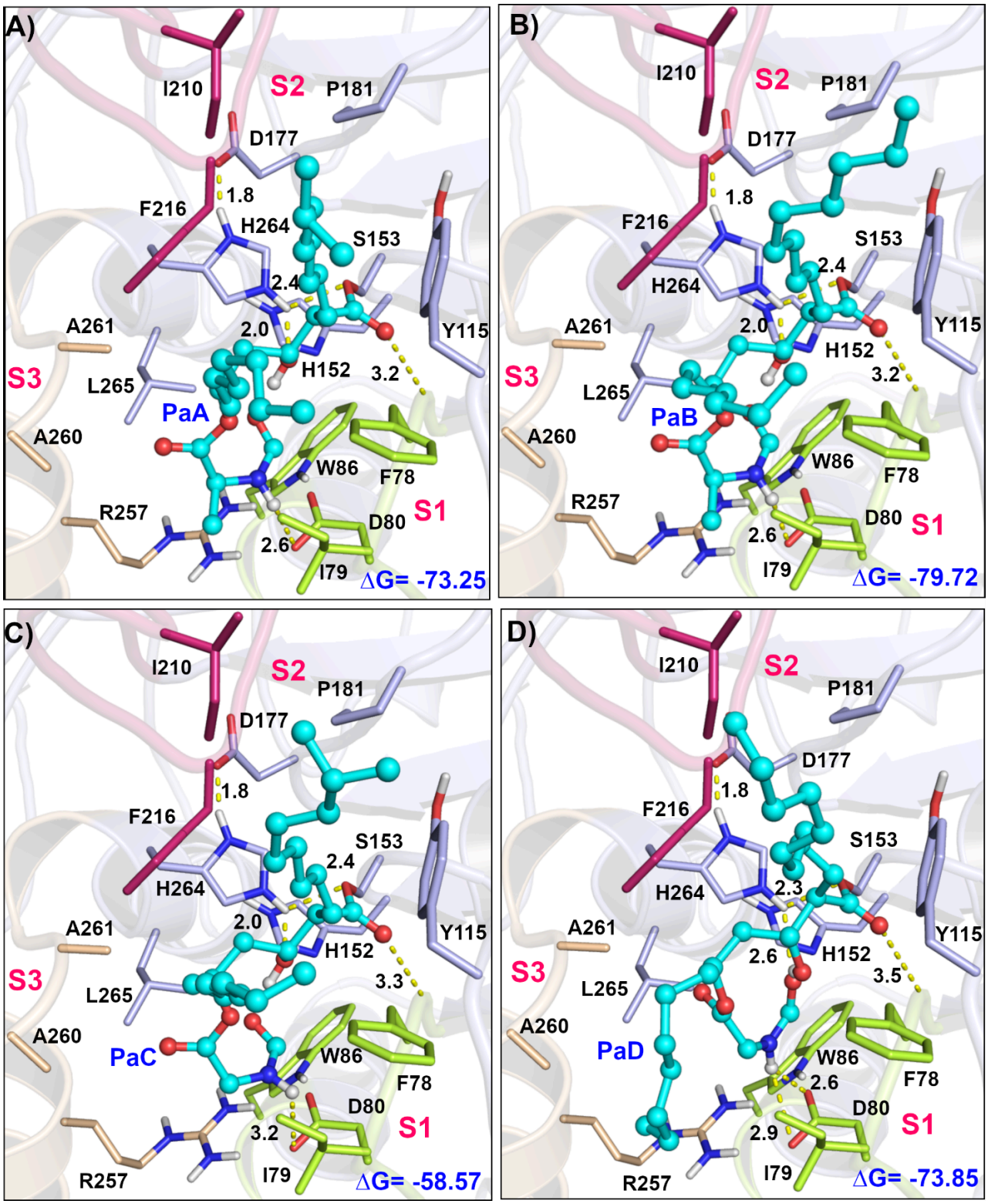


Figure 4

Covalent binding poses of PaA-Panclicin A (A), PaB-Panclicin B (B), PaC-Panclicin C (C), and PaD-Panclicin D (D), in the active site pocket of pancreatic lipase (PL) after a 100 ns metadynamics simulation run. Interacting residues of the pancreatic lipase protein are shown in limon, representing β-5 loop and S1 sub-pocket, warm pink, representing β-9 loop and S2 sub-pocket, in wheat colour, representing lid region or S3 sub pocket. Hydrogen bonding interactions are illustrated with yellow lines.

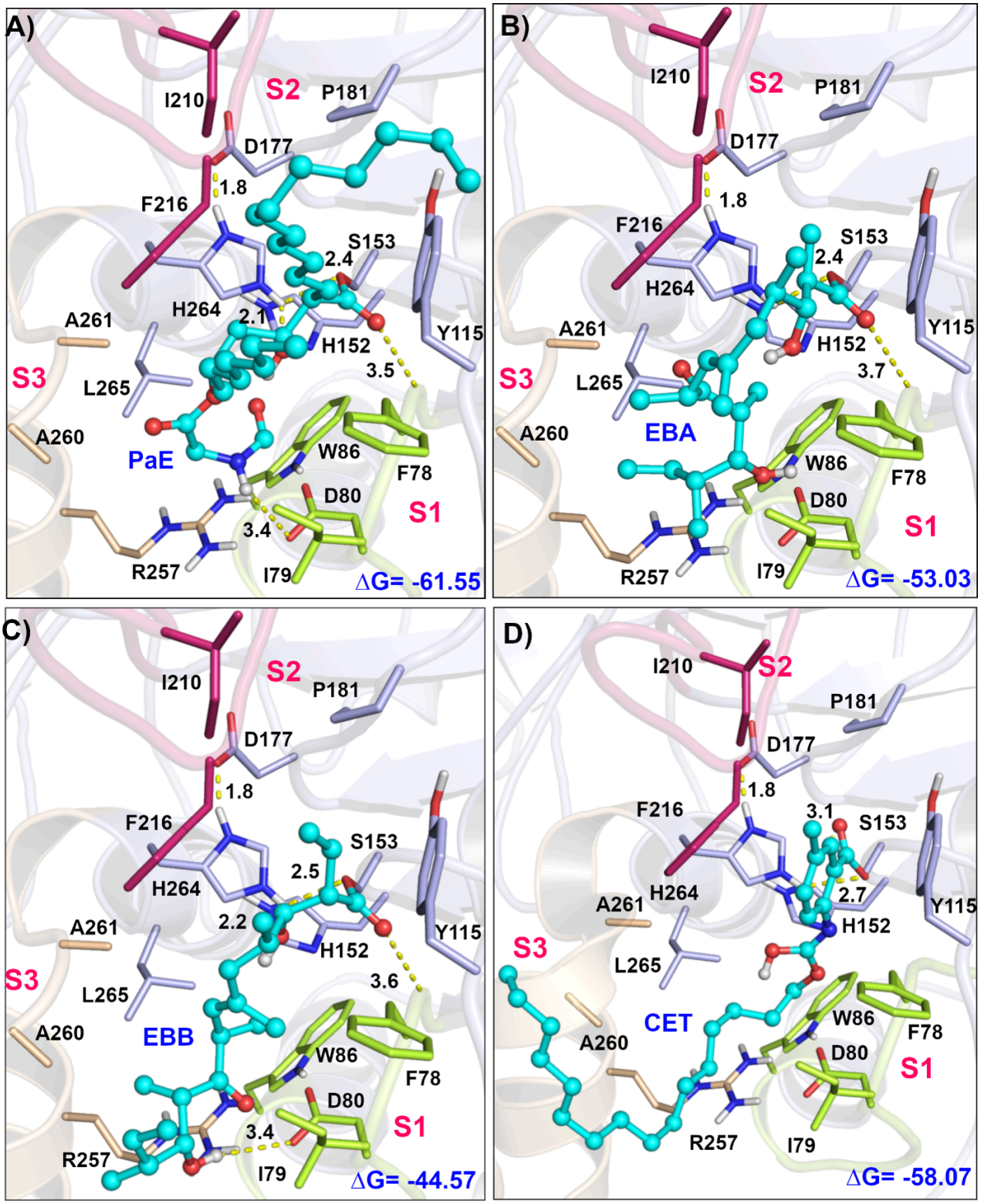


Figure 5

Covalent binding poses of PaE-Panclicin E (A), EBA-Ebelactone A (B), EBB-Ebelactone B (C), and CET-Cetilistat (D), in the active site pocket of pancreatic lipase (PL) after a 100 ns metadynamics simulation run. Interacting residues of the pancreatic lipase protein are shown in limon, representing β-5 loop and S1 sub-pocket, warm pink, representing β-9 loop and S2 sub-pocket, in wheat colour, representing lid region or S3 sub pocket. Hydrogen bonding interactions are illustrated with yellow lines.

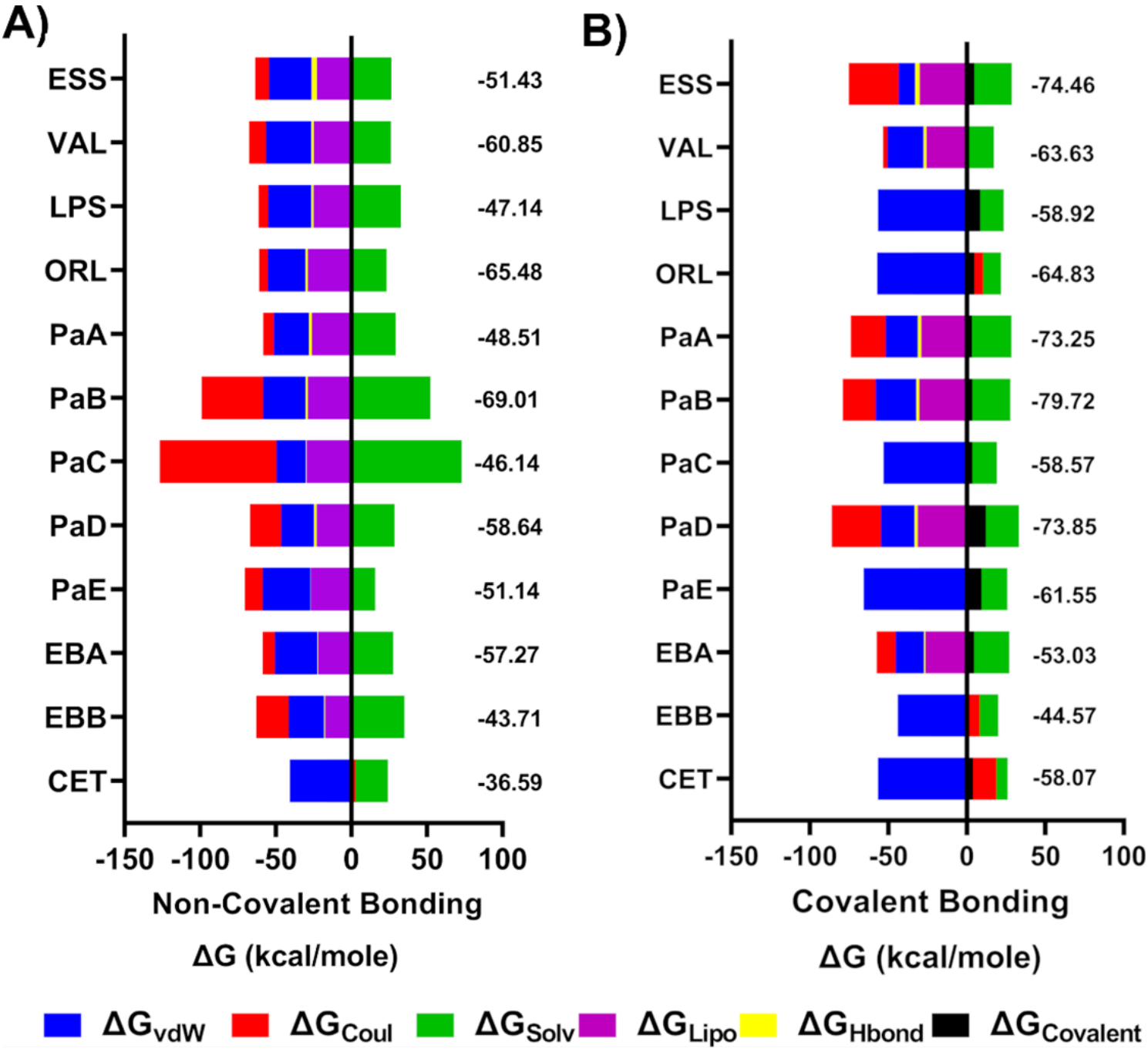


Figure 6

The figure (A) illustrates non-covalent binding energy ($\Delta G_{(MMGBSA)}$ in kcal/mol) and components, including electrostatic, van der Waals, and coulombic energy and lipophilic energy, of lactone inhibitors of pancreatic lipase, ORL-Orlistat, VAL-Valilactone, ESS-Esterastin, LPS-Lipstatin, PaA-Panclicin A, PaB-Panclicin B, PaC-Panclicin C, PaD-Panclicin D, PaE-Panclicin E, EBA-Ebelactone A, EBB-Ebelactone B and CET-Cetilistat. (B) shows the covalent binding energy, which includes all the factors along with covalent energy contribution represented in black. The binding energy represented here, were calculated in OPLS3s forcefield.

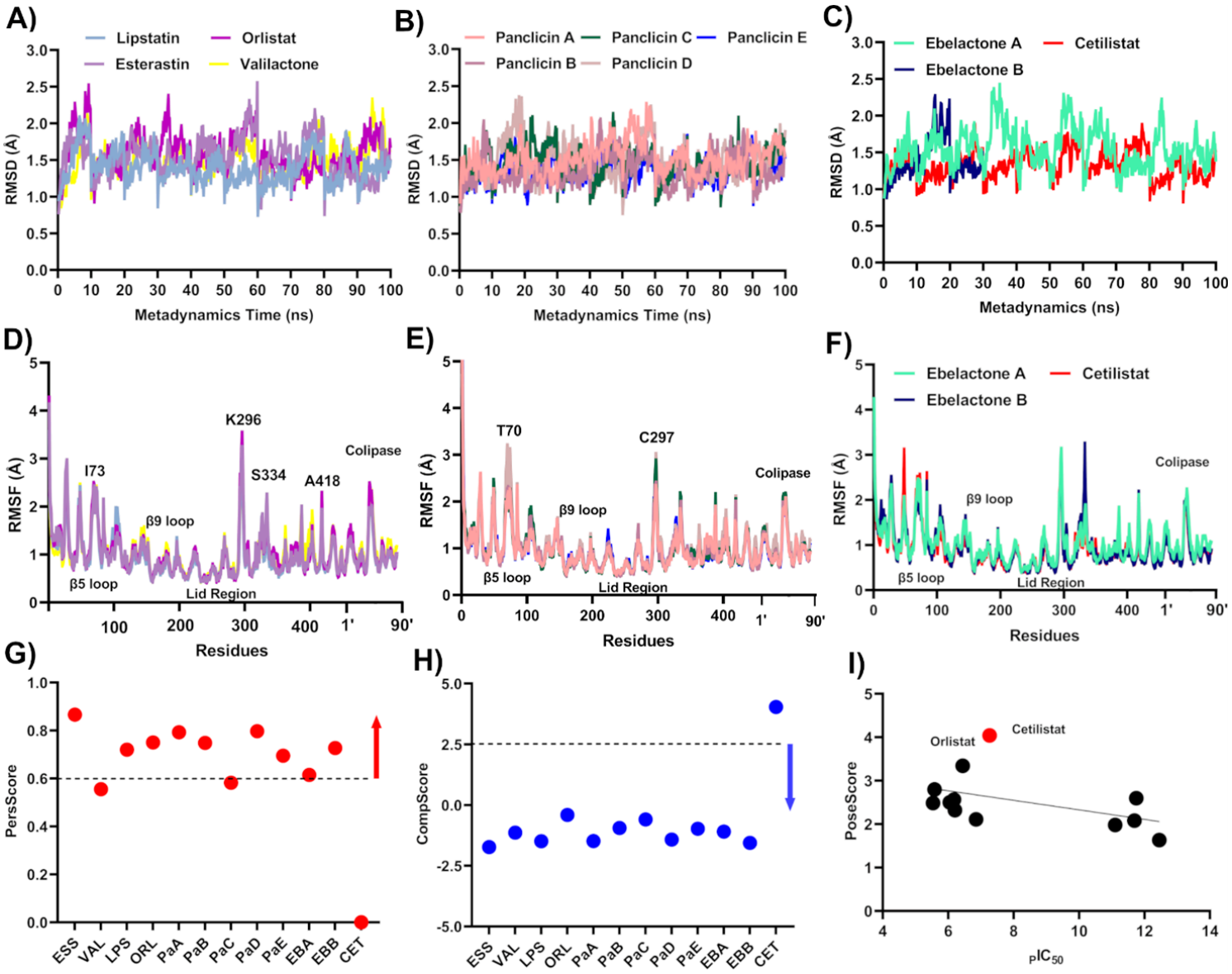


Figure 7

Figure A to C - Root Mean Square Deviation-RMSD, D to E - Root Mean Square Fluctuation-RMSF analyses of PL – Lactone complex, Esterastin, Valilactone, Lipstatin, Orlistat, Panclicin A-E, Ebelectone A and B, and Cetilistat, in different colour codes. (G) represents PerScore indicating the score for crucial interactions with PL active site, (H) illustrating the combined score of PerScore and PoseScore values,

representing the strength of binding, (I) indicates the inverse relationship of stability of the lactones - poses (PoseScore) and their experimental $_{P}IC_{50}$ towards PL. Red dot in (I) is the outlier - Cetilistat.

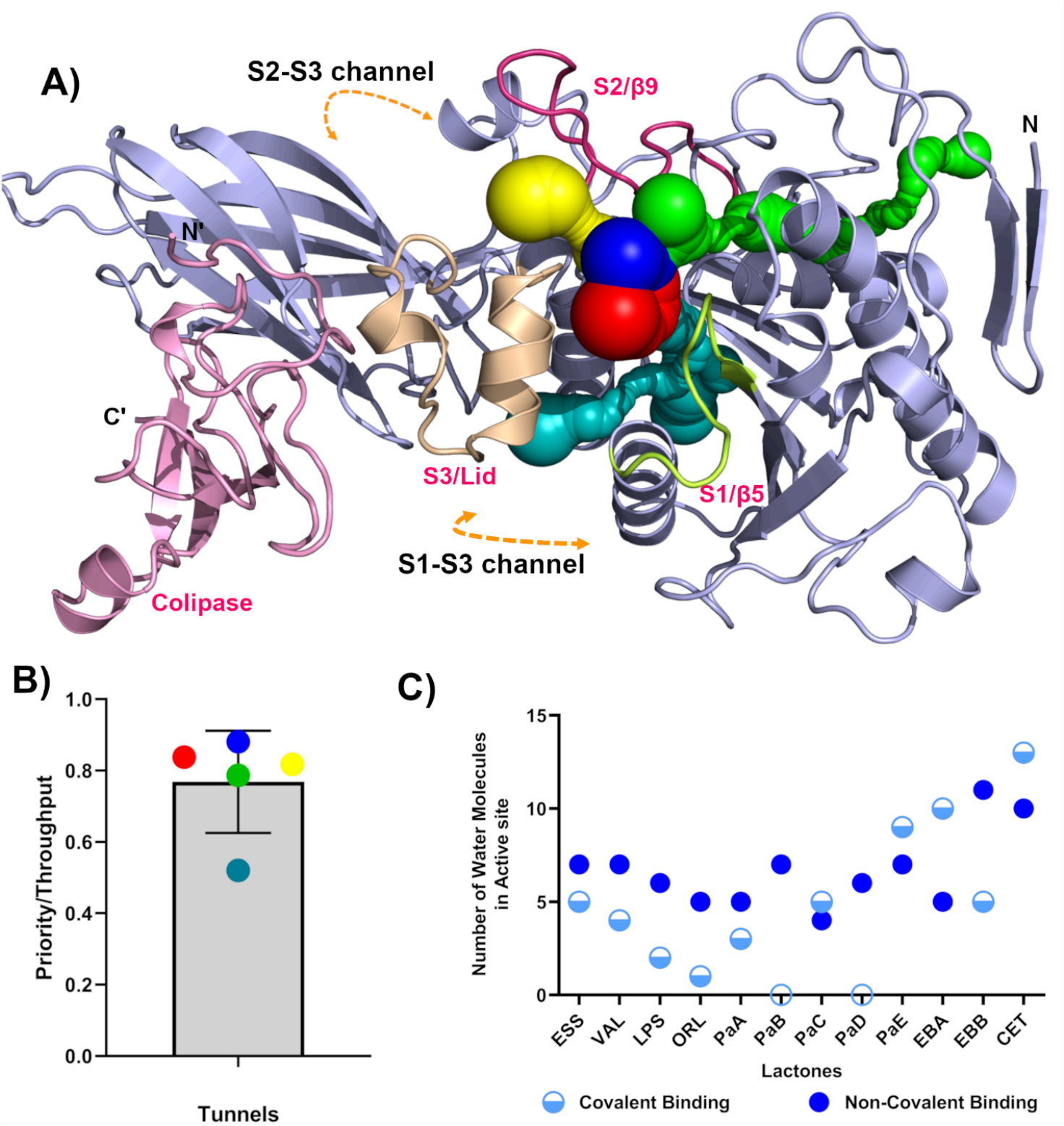


Figure 8

(A) Visualization of water tunnels in apo form of pancreatic lipase (PL), highlights the pathways for water molecules to traverse the protein structure (B) represents their associated priority or throughput values.

(C) represents the number of water molecules present near residue S153, during both non-covalent and covalent binding events over 100 ns of Molecular Dynamics (MD) and well-tempered Metadynamics (wt-metaD) simulations, respectively.

Supplementary Files

This is a list of supplementary files associated with this preprint. Click to download.

- SIPLlactonesJPCB.docx
- GraphicalAbstract.png